The impact of ensemble filter definition
on the assimilation of temperature profiles in the tropical Pacific

By O. LEEUWENBURGH[1]*, G. EVENSEN[2,3] and L. BERTINO[3]
[1]*Royal Netherlands Meteorological Institute (KNMI), De Bilt, the Netherlands*
[2]*Norsk Hydro, Bergen, Norway*
[3]*Nansen Environmental and Remote Sensing Centre, Bergen, Norway*

SUMMARY

The traditional analysis scheme in the Ensemble Kalman Filter (EnKF) uses a stochastic perturbation or randomization of the measurements which ensures a correct variance in the updated ensemble. An alternative so-called deterministic analysis algorithm is based on a square-root formulation where the perturbation of measurements is avoided. Experiments with simple models have indicated that ensemble collapse is likely to occur when deterministic filters are applied to nonlinear problems. In this paper the properties of stochastic and deterministic ensemble analysis algorithms are evaluated in an identical-twin experiment using an ocean general-circulation model. In particular, the implications of the use of deterministic Ensemble Square-Root Filters (EnSRF) for ensemble distribution are investigated. An explanation is presented for the observed collapse, and a simple solution based on randomization of the analysis ensemble anomalies is examined. A one-year assimilation run with this improved EnSRF is found to produce Gaussian distributions, similar to the EnKF.

KEYWORDS: Ensemble Kalman Filter   Ensemble Square-Root Filter

1. INTRODUCTION

The Ensemble Kalman Filter (EnKF) provides a linear update to a nonlinear fore-cast ensemble and can thus be viewed as an intermediate step between the Kalman filter and particle filters (Bertino *et al.* 2003). Investigations into its application to both atmospheric and oceanographic systems have shown significant improvements with respect to optimum-interpolation-type systems (Keppenne and Rienecker 2002; Houtekamer *et al.* 2005), and similar performance as currently operational three-dimensional variational (3D-Var) systems (Houtekamer *et al.* 2005). The stochastic EnKF algorithm (Evensen 1994; Burgers *et al.* 1998) has properties and limitations which are by now well understood. Outstanding issues are primarily related to the maintenance of ensemble spread and balance for relatively small ensemble sizes, and the treatment of model bias.

Some recent studies have promoted deterministic filters on the grounds that they are expected to be more accurate and computationally more efficient, and preserve certain higher-order, non-Gaussian statistics of the forecast ensemble (Tippett *et al.* 2003). Lawson and Hansen (2004) compared the behaviour of the EnKF with the deterministic Ensemble Square-Root Filter (EnSRF) of Whitaker and Hamill (2002) in linear and nonlinear dynamical regimes with simple test models. They noticed that, while ensemble variance is formally maintained by the EnSRF, all members but one tend to collapse onto one state, with a single outlier providing the prescribed variance. The EnKF on the other hand tends to maintain a Gaussian ensemble spread also under nonlinear dynamical regimes due to the Gaussian distribution of the observation perturbations.

The question addressed here is to what extend these findings are relevant for realistic applications with fully nonlinear models based on the primitive equations and relatively small ensemble sizes. In particular, we compare the behaviour of the EnKF and an EnSRF in an identical-twin experiment, where temperature profiles are

---

* Corresponding author: IMAU, Utrecht University, PO Box 80000, 3508 TA, Utrecht, The Netherlands.
e-mail: o.leeuwenburgh@phys.uu.nl

assimilated into the tropical Pacific domain of an ocean general-circulation model (OGCM).

The assimilation algorithms are reviewed briefly in section 2. The addition of a randomization step to the EnSRF algorithm is suggested as a means to counter the tendency for ensemble collapse. Section 3 gives a short overview of the experiment set-up, including a description of the model. Results from one-year assimilation runs with the EnKF, EnSRF, and the randomized EnSRF are presented in section 4. Finally, section 5 concludes with a summary and discussion.

2. ANALYSIS ALGORITHMS

The analysis algorithms discussed here are described in detail by Evensen (2004), but are now reviewed briefly. The EnSRF algorithm is explored in some more detail.

(a) *Ensemble Kalman Filter*

The standard EnKF algorithm (Evensen 1994; Burgers *et al.* 1998) is described by

$$\mathbf{A}^a = \mathbf{A} + \mathbf{PH}^T(\mathbf{HPH}^T + \mathbf{R})^{-1}(\mathbf{D} - \mathbf{HA}) \tag{1}$$

$$= \mathbf{A} + \mathbf{A}'\mathbf{A}'^T\mathbf{H}^T\{\mathbf{HA}'\mathbf{A}'^T\mathbf{H}^T + (N-1)\mathbf{R}\}^{-1}(\mathbf{D} - \mathbf{HA}), \tag{2}$$

where $\mathbf{A} = (\boldsymbol{\psi}_1, \ldots, \boldsymbol{\psi}_N)$ holds the ensemble of model forecasts, $\mathbf{H}$ is the measurement operator, $\mathbf{R}$ is the observation error covariance matrix, and $\mathbf{D}$ is the ensemble of perturbed measurements. Primes indicate anomalies with respect to the ensemble mean, and the ensemble covariances are defined by $\mathbf{P} = \mathbf{A}'\mathbf{A}'^T/(N-1)$, where N is the ensemble size and the superscript T indicates the matrix transpose.

(b) *Ensemble Square-Root Filter*

The EnSRF updates the ensemble mean and the anomalies separately. The updated mean, $\overline{\boldsymbol{\psi}^a}$, is computed by an equation similar to Eq. (1), i.e.

$$\overline{\boldsymbol{\psi}^a} = \overline{\boldsymbol{\psi}^f} + \mathbf{PH}^T(\mathbf{HPH}^T + \mathbf{R})^{-1}(\mathbf{d} - \mathbf{H}\overline{\boldsymbol{\psi}^f}), \tag{3}$$

where $\mathbf{d}$ are the unperturbed measurements. This gives exactly the same updated ensemble mean as the EnKF as long as the measurement perturbations average to zero.

An equation for the updated perturbations is obtained by analogy between the definition of the ensemble covariance matrix and the updated covariance, which follows from Kalman Filter theory rewritten as the square of two matrices:

$$(N-1)\mathbf{P}^a = \mathbf{A}^{a'}\mathbf{A}^{a'T} = (N-1)\mathbf{P}\{\mathbf{I} - \mathbf{H}^T(\mathbf{HPH}^T + \mathbf{R})^{-1}\mathbf{HP}\} \tag{4}$$

$$= \mathbf{A}'(\mathbf{I} - \mathbf{S}^T\mathbf{C}^{-1}\mathbf{S})\mathbf{A}'^T \tag{5}$$

$$= \mathbf{A}'(\mathbf{I} - \mathbf{Z}\boldsymbol{\Lambda}\mathbf{Z}^T)\mathbf{A}'^T \tag{6}$$

$$= \mathbf{A}'\mathbf{Z}(\mathbf{I} - \boldsymbol{\Lambda})\mathbf{Z}^T\mathbf{A}'^T \tag{7}$$

$$= (\mathbf{A}'\mathbf{Z}\sqrt{\mathbf{I} - \boldsymbol{\Lambda}})(\mathbf{A}'\mathbf{Z}\sqrt{\mathbf{I} - \boldsymbol{\Lambda}})^T. \tag{8}$$

The notation $\mathbf{S} = \mathbf{HA}'$ and $\mathbf{C} = \mathbf{SS}^T + (N-1)\mathbf{R}$ is introduced in Eq. (5) and an eigen-value decomposition of the second term within the brackets of Eq. (5) is computed to obtain the eigenvectors $\mathbf{Z}$ and eigenvalues $\boldsymbol{\Lambda}$ (see Evensen 2004 for details). Thus a

particular solution for the ensemble perturbations is:

$$\mathbf{A}^{\mathrm{a}\prime} = \mathbf{A}^{\prime}\mathbf{Z}\sqrt{\mathbf{I} - \boldsymbol{\Lambda}}. \tag{9}$$

This is essentially the same equation as is solved in the EnSRF algorithms discussed in Tippett *et al.* (2003), although they introduced additional simplifications for computational reasons.

At this point it becomes clear that the classification of the EnSRF as a 'deterministic method' is slightly misleading. First of all, we note that the above solution is not unique, but only one from many possible solutions. Furthermore, the sign of the eigenvectors $\mathbf{Z}$ is arbitrary. If the physical model is nonlinear, choosing the opposite sign will eventually lead to a different result in the data assimilation experiment.

A problem with the square-root filter algorithm can be illustrated by a simple example where a single observation is used with a scalar state. With a direct measurement operator $\mathbf{H} = 1$ we have $\mathbf{S} = \mathbf{A}^{\prime}$. Further, since only the first eigenvalue in $\boldsymbol{\Lambda}$ is non-zero, then the first eigenvector in $\mathbf{Z}$ must be identically proportional to $\mathbf{S}^{\mathrm{T}}$. (Note that we have $\mathbf{S} \in \Re^{1 \times N}$ in the case with a single measurement.) This is seen from the equality between Eqs. (5) and (6). However, all the remaining $N - 1$ eigenvectors are orthogonal to the first eigenvector, and thus also orthogonal to $\mathbf{S}^{\mathrm{T}}$.

Thus, the update Eq. (9) will lead to an ensemble of updated perturbations where the first member will be equal to $\mathbf{S}(\mathbf{S}^{\mathrm{T}}/\|\mathbf{S}\|)\sqrt{1 - \lambda_1}$ and all the $N - 1$ remaining perturbations will be identical to zero. Note that the resulting ensemble still has the correct variance, but it is determined by the perturbation in the first ensemble member.

This example can clearly be extended to cases with larger state spaces. For example, if the state dimension $n > 1$, there will still be a problem at the measurement locations. In fact the rank of the ensemble is reduced to one at the measurement location.

With more than one measurement, the situation changes slightly but the same problem will occur if $\mathbf{C}^{-1}$ is diagonal. Then each of the m columns in $\mathbf{S}^{\mathrm{T}}$ will be proportional to one of the first m eigenvectors in $\mathbf{Z}$. Thus, the first m ensemble perturbations will represent the analysis variance while the remainder will be zero. More generally, the norm of the ensemble perturbations in Eq. (9) is dependent on the eigenvalue spectrum $\boldsymbol{\Lambda}$ which can be strongly asymmetric.

This explains the findings of Lawson and Hansen (2004), where it was shown that the EnSRF tends to produce ensembles where the variance is provided by very few outliers.

The problem sketched here can be avoided by the insertion of a random orthogonal matrix product $\mathbf{I} = \mathbf{V}^{\mathrm{T}}\mathbf{V}$ in Eq. (8), as was proposed by Evensen (2004), i.e.

$$\mathbf{A}^{\mathrm{a}\prime}\mathbf{A}^{\mathrm{a}\prime\mathrm{T}} = \mathbf{A}^{\prime}\mathbf{Z}\sqrt{\mathbf{I} - \boldsymbol{\Lambda}}\mathbf{V}^{\mathrm{T}}\mathbf{V}(\mathbf{A}^{\prime}\mathbf{Z}\sqrt{\mathbf{I} - \boldsymbol{\Lambda}})^{\mathrm{T}}, \tag{10}$$

which leads to the randomized EnSRF update equation

$$\mathbf{A}^{\mathrm{a}\prime} = \mathbf{A}^{\prime}\mathbf{Z}\sqrt{\mathbf{I} - \boldsymbol{\Lambda}}\mathbf{V}^{\mathrm{T}}. \tag{11}$$

The multiplication with $\mathbf{V}^{\mathrm{T}}$ is equivalent to a random rotation of the eigenvectors in $\mathbf{Z}$, which has the effect of randomly distributing the variance among all the ensemble members. The result is still a square root of the updated covariance as in Eq. (4). The random orthogonal matrix $\mathbf{V}^{\mathrm{T}}$ is easily constructed from a singular-value decomposition of a random matrix $\mathbf{B} \in \Re^{N \times N}$, i.e. $\mathbf{B} = \mathbf{U}\boldsymbol{\Sigma}\mathbf{V}^{\mathrm{T}}$.

(c) *Localization*

Following common practice, a covariance localization step was added to the EnKF to reduce long-range spurious correlations and increase the dimension of the solution

space (Houtekamer and Mitchell 2001). The cut-off ranges for the localizing function were 60° and 30° in the zonal and meridional directions respectively and are identical to those chosen by Keppenne and Rienecker (2002). Localization was achieved for the EnSRF without covariance filtering by reducing the data selection ranges for each grid point to 30° and 15° respectively, resulting in an approximately equivalent effective number of observations as for the EnKF.

3.   EXPERIMENT SET-UP

The ocean model that is used here is the Max Planck Institut für Meteorologie Ocean Model, or MPI-OM (Marsland *et al.* 2003). The model is run in a global configuration with meridional refinement of the grid (0.5°) within a 20° latitude band centred on the equator.

The true ocean state is defined by a forward run of the ocean model using NCEP/NCAR* re-analysis forcing fields.

An unconstrained control run is forced with the ECMWF 45-year re-analysis (ERA-40) forcing fields. The use of two different forcing products is meant to reflect the errors in our best-guess forcing products with respect to the true forcing. The initial ensemble at the start of the assimilation run consists of 64 model states which are obtained by a 1-year spin-up of an ensemble with perturbed ERA-40 forcing using the control state as initial condition. The perturbations are determined as temporally correlated random combinations of the dominant empirical orthogonal functions of a 2-year time series of ERA-40–ERA-15 differences. A seasonal cycle was first removed from these differences. Further details of the perturbation method can be found in Leeuwenburgh (2005).

Temperature measurements were simulated by sampling the truth run at the geographical positions of the Tropical Atmosphere–Ocean (TAO) buoys and the corresponding depths of the temperature sensors. Random perturbations with a 1 degC standard deviation were added to all measurements to simulate realistic data errors.

Three assimilation runs lasting 12 months were performed with the EnKF, the EnSRF, and the EnSRF with an additional random rotation step (referred to as EnSRF+). Each run consists of consecutive 10-day forward integrations of the ensemble using perturbed forcing (the resulting mean states being referred to as the *forecasts*), each followed by an update during which the simulated observations are assimilated into the ensemble.

In the following sections the mean states of the resulting ensembles (the *analyses*) will be compared with the control and the truth to determine whether the assimilation has brought the model closer to the true state. The ensemble statistics resulting from the runs are compared to study the characteristics of the ensembles.

4.   RESULTS FROM ASSIMILATION RUNS

(a)   *Ensemble mean states*

Figures 1 and 2 show the mean control and analysis errors averaged over the 12-month assimilation period. (The results from the EnSRF+ were very similar to those from the EnSRF and are not shown.) The large-scale bias in temperature (Fig. 1) has been markedly reduced by the assimilation relative to the control. The EnKF has been more effective in this respect than the EnSRF. The improvement of the temperature field

---

* US National Centers for Environmental Prediction/National Center for Atmospheric Research.
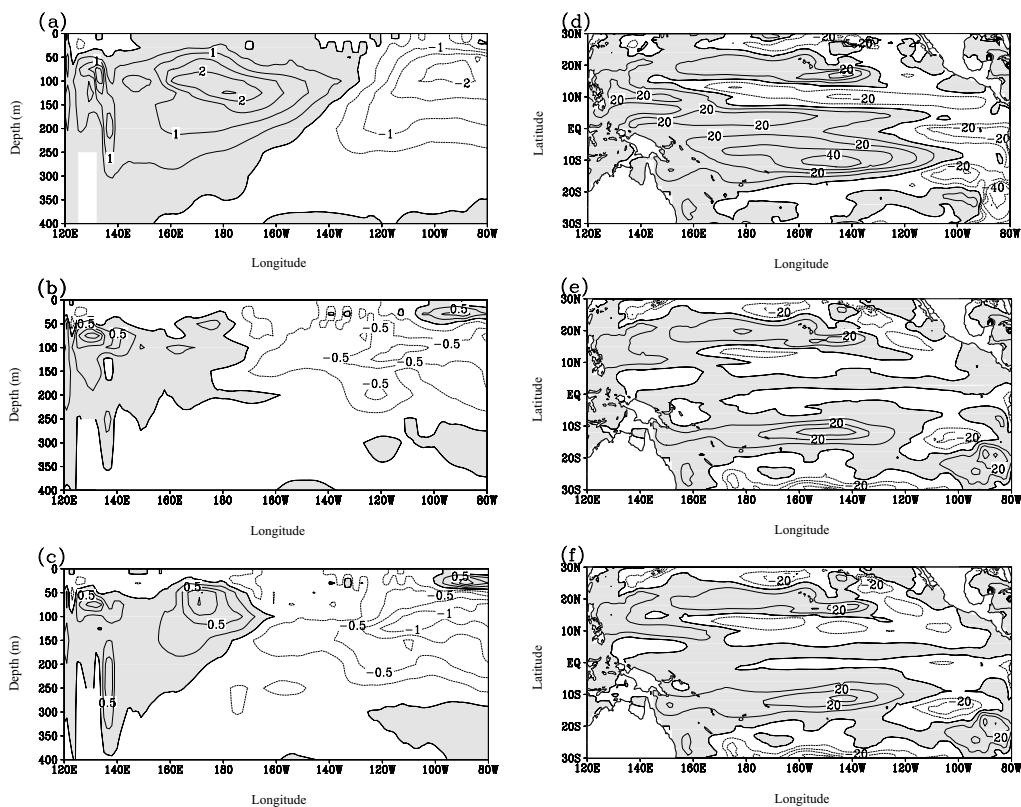
Figure 1.   Errors in temperature (K) along the equator, defined as differences from the truth, for (a) the control, (b) the EnKF, and (c) the EnSRF. Errors in the depth (Z20, m) of the 20 °C contour over the tropics for (d) the control, (e) the EnKF, and (f) the EnSRF. Negative contours are dashed in all cases.

is reflected by the reduction in the error in the position of the thermocline, as indicated here by the depth of the 20 °C isotherm. A similar improvement is seen in the zonal velocities of the Equatorial Under Current (Fig. 2), although in this case the remaining bias appears to be slightly larger for the EnKF than for the EnSRF. The results from the control run show significant errors in the depth profile of vertical velocity along the equator, especially at 100°W where vertical velocity errors of up to 1.5 m day^{-1} can be found. In the EnKF analyses in particular, this upwelling has been strongly reduced, but the reduction appears to be associated with a large-scale overturning circulation with upwelling west of 160°W, and downwelling to the east. The changes in the velocity profile resulting from the EnSRF are less pronounced.

These results were also compared with those resulting from the assimilation of altimetry (Leeuwenburgh 2005). It was found (not shown) that the EnKF analyses resulting from temperature assimilation are consistently better than those resulting from sea-level assimilation, while the EnSRF analyses are of comparable quality.

Some additional summary statistics for sea-level analyses in the standard Niño boxes and temperature forecasts averaged over all observation locations are presented in Table 1. The sea-level and temperature bias estimates largely confirm the picture presented by Fig. 1; biases are significantly reduced by the assimilation, with the exception of sea level in the Niño3.4 region. This is also the only case where the bias from the EnSRF is smaller than that from the EnKF. The consistency between the a priori
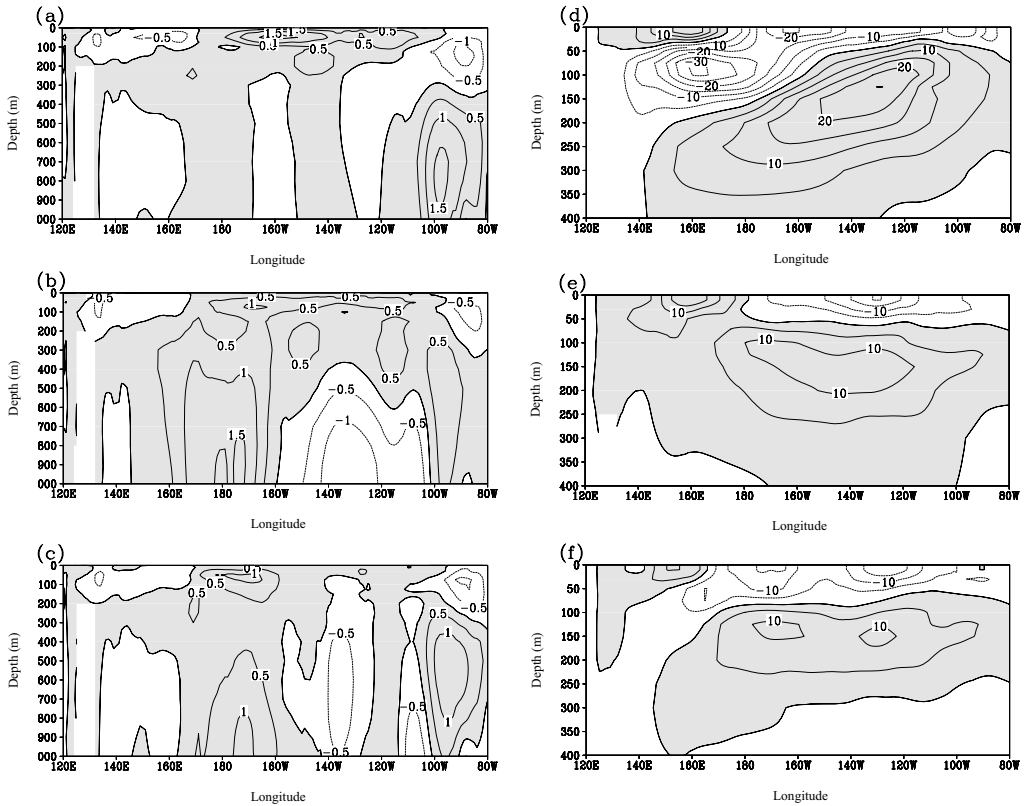
Figure 2.   As Fig. 1(a)–(c), but for (a)–(c) vertical velocity (m day^{-1}), and for (d)–(f) zonal speed (cm s^{-1}).

TABLE 1.   SEA-LEVEL ANALYSIS AND TEMPERATURE FORECAST ERROR STATISTICS

	Niño1+2		Niño3.4		Niño3		Niño4		T	
	bias	r.m.s.e.	bias	r.m.s.e.	bias	r.m.s.e.	bias	r.m.s.e.	bias	r.m.s.e.
Control	−6.6	1.2	1.2	2.9	−3.2	1.7	5.4	2.5	0.83	0.58
EnKF	−1.8	1.0	−2.6	1.2	−2.3	0.7	−2.9	1.7	0.04	0.37
EnSRF	−2.4	1.0	−2.2	1.8	−2.5	0.9	−2.3	2.3	0.17	0.41

Sea-level analysis statistics (cm) are for four standard Niño areas: Niño1+2 = 80–90°W, 0–10°S; Niño3.4 = 120–170°W, 5°S–5°N; Niño3 = 90–150°W, 5°S–5°N; Niño4 = 150°W–160°E, 5°S–5°N. Temperature forecast statistics (K) are for all observation locations.

uncertainty in the forecast and observations was also determined. If it is assumed that forecasts and observations are independent, then the r.m.s. of the forecast–observation differences (determined here after removing a time-mean bias) should be approximately equal to the root of the summed forecast and observation error variances. The average ratio between the two measures over all assimilation steps and all observation locations was 0.94 for the EnKF and 0.97 for the EnSRF. We thus conclude that there is no indication of incorrect specification of ensemble variance or observation error.

While assimilation has resulted in an improved subsurface temperature field, it is clear that significant biases remain, and also that systematic errors are introduced in the vertical transports of the model. Bell *et al.* (2004) have shown that these systematic errors may appear as the result of combining a model driven by poorly known winds with
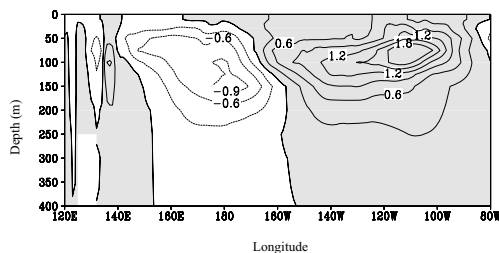
Figure 3.   Mean temperature increment (K month^{-1}).

high-quality density information. Errors in the large-scale winds will be accompanied by compensating errors in the subsurface density field. Assimilation will correct the subsurface density field, thereby simultaneously disturbing the balance between the surface pressure and wind stress, resulting in spurious circulations that tend to restore this balance. Figure 3 shows the temperature increment along the equator averaged over all assimilation steps during the one-year run. The large-scale pattern of heating and cooling shows that the model is not in dynamical balance but consistently drifts away from the assimilated state during the forecast (Bell *et al.* 2004). In the following we have chosen an approach that is independent of bias and allows a clean assessment of the ensemble distributions.

(b)   Ensemble distribution

Figure 4 shows time series of the analysed temperature at one of the measurement locations for all three runs. The small dots in these figures show the distribution of the individual members of the analysis ensembles. The three important observations that can be made from this figure are that (i) the EnSRF produces the same behaviour that was observed by Lawson and Hansen (2004), with in most cases only one outlier apparently providing the required variance; (ii) the random rotation in the randomized version EnSRF+ produces an ensemble with a more even spread; and (iii) the spread in the EnSRF+ members appears to be slightly less than for the EnKF.

The shape of the ensemble distribution can be assessed quantatively using the skewness measure which is an indication of the asymmetry around the mean. Since a Gaussian distribution is symmetric, high skewness values indicate strong deviations from a Gaussian shape. The skewness of temperature values is determined at all measurement locations and at all time steps. Figure 5 shows for all three algorithms the resulting minimum and maximum values, the median, and the interquartile ranges found during each run. While the skewness values are very low for the EnKF and the EnSRF+, high values are obtained for the EnSRF, in agreement with the indications from the time series of Fig. 4. Since the forecast skewness estimates indicate fairly symmetric distributions, these high values must be an artefact of the EnSRF analysis algorithm.

Lawson and Hansen (2004) produced rank histograms as an additional tool to illustrate the high number of outliers. Hamill (2001) showed that rank histograms may indicate several deficiencies of the ensemble simultaneously, one of them being conditional biases which result in U-shaped histograms similar to those shown by Lawson and Hansen (2004). It was shown earlier that biases do indeed remain in the analysis. Rank histograms may therefore not be the optimal tool for assessment of the ensemble distribution in this case. Instead, a χ^2 test is performed here to determine
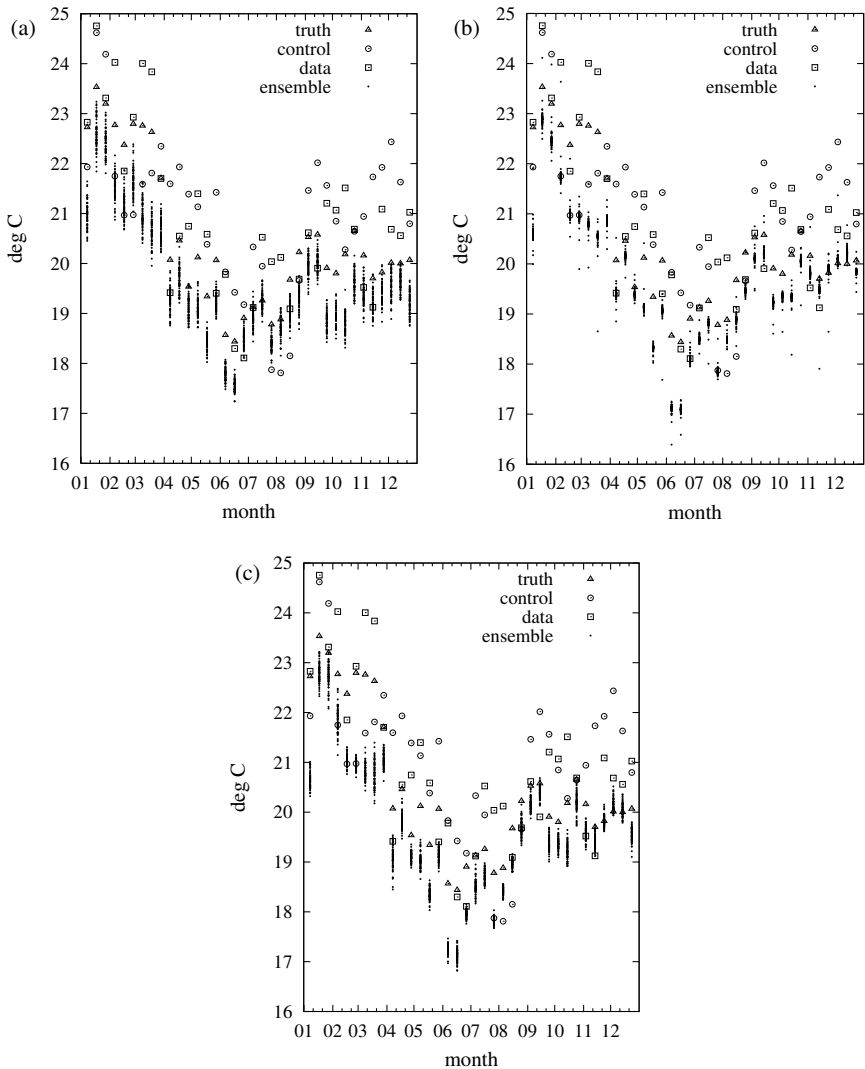
Figure 4.   Temperature values at 120 m depth at 220°E, 0°N from the truth, control, observations, and the
ensembles obtained with (a) the EnKF, (b) the EnSRF, and (c) the EnSRF with rotation.

whether the distributions are Gaussian or not. The temperature samples shown in Fig. 4
were binned into 6 classes relative to the ensemble mean values, each representing an
equal area of the Gaussian probability density function corresponding to the estimated
standard deviation of ensemble spread. The sum of the squared differences between
the number of occurrences in each class and the expected value (64/6) has a χ^2
distribution. The corresponding *p*-values are determined at every time step during the
assimilation run. If the number of rejections of the Gaussian assumption, following
from all individual χ^2 tests, exceeds a critical number associated with the binomial
distribution and a chosen significance level, we conclude that the ensemble distributions
are non-Gaussian. For the time series of Fig. 4, the Gaussian null-hypothesis is rejected
at every time step for the EnSRF. The number of rejections for the EnKF and EnSRF+
is low enough that we can state with a 95% confidence level that the distributions are
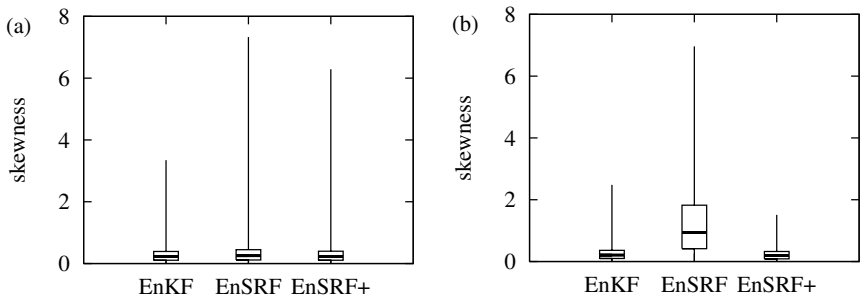Gaussian.

Figure 5.   Ensemble skewness determined at observations points for (a) the forecast ensembles and (b) the analysis ensembles resulting from the assimilation runs with EnKF, EnSRF and EnSRF with rotation (EnSRF+). The thick line indicates the median value, the box bounds indicate the interquartile range, and the whiskers extend to the min and max values. The maximum theoretical value is 7.75.

5.   DISCUSSION AND CONCLUSIONS

Experiments are conducted to compare the behaviour of so-called stochastic and deterministic ensemble filters in a realistic application. Simulated tropical temperature profiles are assimilated in an OGCM using Ensemble Kalman and Square-Root Filters. The mean analysed states produced with the EnKF are generally slightly better than those from the EnSRF except in the Niño3.4 region. In agreement with Lawson and Hansen (2004), we find that the EnSRF has a tendency to collapse all but a few members onto a single state. Skewness measures and χ^2 tests confirm that the resulting ensembles are highly non-Gaussian and that the non-Gaussianity is introduced by the EnSRF analysis scheme.

These findings point to some fundamental problems with the EnSRF. Members of an ensemble should be equally likely, but the EnSRF updated anomalies are aligned on singular vectors representing unequal contributions to the total variance. Members associated with small eigenvalues are almost equal to the mean, and therefore useless in the ensemble. The skewness observed with the EnSRF is most likely inherited from the skewness of the singular-values spectrum (many near-zero singular values, few large values).

The EnSRF reduces errors along specific directions defined by $\mathbf{Z}$ in Eq. (9), where $\mathbf{Z}$ is a rotation which comes from the singular-value decomposition of the product of the eigenvectors of $\mathbf{C}$ and $\mathbf{S}$. Dependent on this product, it is not clear what this will mean in different situations. The single observation and diagonal $\mathbf{C}$ cases are just two cases where problems arise, and there may be more. In fact, even though all observations were assimilated simultaneously at each step, and a diagonal $\mathbf{C}$ is unlikely to occur in realistic applications in oceanography and meteorology, similar behaviour was found to occur in our experiments. An additional random rotation of the ensemble anomalies is found to fix the above problems well.

The EnSRF+ analysis scheme is deterministic in the sense that the updated mean and covariance strictly comply to the Kalman Filter equations. The EnKF only achieves this asymptotically with an infinite number of members. In our experiments however, the EnKF performs slightly better than the EnSRF+. This shows that the exigence of respecting exactly the Kalman Filter mean and covariance may be a worthy objective but not the only key to the success of an assimilation algorithm. Differences between the EnKF and the EnSRF+ in this particular experiment may be linked either to the

conservation of higher-order statistics or to the conservation of physical properties. These differences will need deeper examination before they can be generalized to other geophysical systems.

REFERENCES

Bell, M. J., Martin, M. J. and Nichols, N. K. — 2004 — Assimilation of data into an ocean model with systematic errors near the equator. *Q. J. R. Meteorol. Soc.*, **130**, 873–893

Bertino, L., Evensen, G and Wackernagel, H. — 2003 — Sequential data assimilation techniques in oceanography. *Int. Stat. Rev.*, **71**(2)**,** 223–241

Burgers, G., van Leeuwen, P. J. and Evensen, G. — 1998 — Analysis scheme in the Ensemble Kalman Filter. *Mon. Weather Rev.*, **126**, 1719–1724

Evensen, G. — 1994 — Sequential data assimilation with a nonlinear quasi-geostrophic model using Monte Carlo methods to forecast error statistics. *J. Geophys. Res.*, **C99,** 10143–10162

— 2004 — Sampling strategies and square root analysis schemes for the EnKF. *Ocean Dyn.*, **54**, 539–560

Hamill, T. M. — 2001 — Interpretation of rank histograms for verifying ensemble forecasts. *Mon. Weather Rev.*, **129**, 550–560

Houtekamer, P. and Mitchell, H. L. — 2001 — A sequential Ensemble Kalman Filter for atmospheric data assimilation. *Mon. Weather Rev.*, **129**, 123–137

Houtekamer, P., Mitchell, H. L., Pellerin, G., Buehner, M., Charron, M., Spacek, L. and Hansen, B. — 2005 — Atmospheric data assimilation with an Ensemble Kalman Filter: results with real observations. *Mon. Weather Rev.*, **133**, 604–620

Keppenne, C. L. and Rienecker, M. M. — 2002 — Initial testing of a massively parallel Ensemble Kalman Filter with the Poseidon isopycnal ocean general circulation model. *Mon. Weather Rev.*, **130**, 2951–2965

Lawson, W. G. and Hansen, J. A. — 2004 — Implications of stochastic and deterministic filters as ensemble-based data assimilation methods in varying regimes of error growth. *Mon. Weather Rev.*, **132**, 1966–1981

Leeuwenburgh, O. — 2005 — Assimilation of along-track altimeter data in the tropical Pacific region of a global OGCM ensemble. *Q. J. R. Meteorol. Soc.*, **131**, 2455–2472

Marsland, S., Haak, H., Jungclaus, J. H., Latif, M. and Röske, F. — 2003 — The Max-Planck-Institute global ocean/sea ice model with orthogonal curvilinear coordinates. *Ocean Modelling*, **5,** 91–127

Tippett, M. K., Anderson, J. L., Bishop, C. H., Hamill, T. M. and Whitaker, J. S. — 2003 — Ensemble square-root filters. *Mon. Weather Rev.*, **131**, 1485–1490

Whitaker, J. S. and Hamill, T. M. — 2002 — Ensemble data assimilation without perturbed observations. *Mon. Weather Rev.*, **130**, 1913–1924